POLITECNICO DI TORINO
Repository ISTITUZIONALE

Analysis of Integrated Optics Parametric Oscillators Characteristics

(Article begins on next page)

11 April 2024

Analysis of Integrated Optics Parametric Oscillators

G. Colucci, D. Romano, Gian Paolo Bava, and Ivo Montrosset

Abstract—An almost analytical model for the analysis of integrated optics parametric oscillators is proposed. A comprehensive discussion of the static device characteristics of a doubly resonant oscillator varying the parameters of the optical cavity which influence the operation conditions (single, double pass and resonant pump) is presented. A detailed discussion of the evolution towards the singly resonant condition and the possibility of hysteretic behaviour is also included.

I. INTRODUCTION

INTEREST in parametric phenomena, from microwave to optical wavelengths, is well established and is concerned with the possibility of generating, amplifying, and detecting signals in frequency ranges where it is not easy to operate by other means [1]-[3]. More recently the development of optical mixing effects under guided wave conditions [4]-[6] has increased the range of application, owing to the rather small pump power required with such working conditions. The principles of operation of optical parametric devices, the main operating characteristics, and the possible applications are treated in several review papers [3], [6]-[9]. The aim of the present paper is to numerically model integrated optics parametric oscillators (IOPO), taking into account realistic parameters and operating conditions. This is a laborious task, if we use a full numerical approach, due to the multiple frequency operation and the large number of parameters needed to describe the device and operating conditions. Hence, we present a model, based on the high quality factor assumption, which allows an almost analytical solution of wide generality, whose implementation does not require a large computational effort. In this way it is possible to carry out an exhaustive analysis of parametric oscillator characteristics.

A number of numerical results are reported and the influence of several device parameters are discussed. The results are mainly concerned with the doubly resonant IOPO, for which comparisons with experimental data are easier to make. The evolution towards singly resonant operation is also discussed. However, to take into account realistic operating conditions, single and double pump pass configurations are also considered as that of the resonant pump.
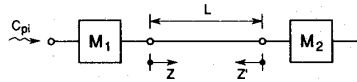
Fig. 1. Schematic structure of the parametric oscillator cavity.

II. PARAMETRIC OSCILLATOR MODEL

The structure of the considered parametric oscillator is represented in Fig. 1 where c_{pi} represents the incident pump amplitude, L is the cavity length, and M_1, M_2 are the input and output mirrors.

It is well known that the operating conditions of a doubly resonant parametric oscillator are strongly influenced by three requirements.

1) The parametric gain bandwidth, which imposes a limitation on the range of values of the mismatch

$$\Delta\beta L = (\beta_p - \beta_s - \beta_i)L \qquad (1)$$

β being the propagation constant for pump, signal, and idler waves, respectively.

2) The energy conservation relation

$$\omega_p = \omega_s + \omega_i. \qquad (2)$$

3) The simultaneous requirement of resonance at both signal and idler, that is

$$\beta_s L \cong p\pi, \quad \beta_i L \cong q\pi \qquad (3)$$

where, for simplicity, the phase introduced by the mirrors has not been written explicitly and $\cong$ means operation inside the cavity resonance; p and q are integer values. The last condition gives rise to the well-known "cluster problem" [10], [11]. Here, the possible operating conditions are grouped in one or more clusters, inside the gain region, where relations (3) are more closely satisfied (see Fig. 2). This condition, at least for high Q resonators, is very restrictive.

It has been shown, both experimentally and by numerical simulations [12], [13], that single frequency IOPO operation (at signal and idler) can be achieved in the range of parameter values where only one cluster occurs. This is due to the need for almost complete overlapping of the nearest resonances at signal and idler in order to satisfy (3).

Referring to Fig. 3, by using β_s and β_i scales, such that points on the vertical satisfy exact energy conservation a possible operating condition is shown along with the shifts $\Delta\beta_s$ and $\Delta\beta_i$ from the working point (•) with respect to the free resonances.
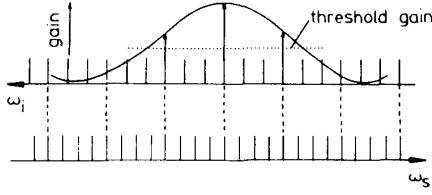
Fig. 2. Parametric gain curve versus ω_s and ω_i for given ω_p; the scales are drawn so that (2) is satisfied. Vertical lines represent the free cavity resonances.
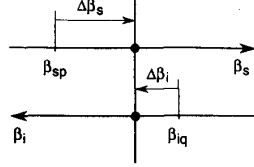

Fig. 3. Region of interest for single frequency emission (the two nearest resonances for signal and idler are represented together with the working point •).

The relation between $\Delta\beta_s(\Delta\beta_i)$ and the corresponding $\Delta\omega_s(\Delta\omega_i)$, for small shifts, is obtained through the group velocity of the propagating modes:

$$\Delta\omega_s = v_{gs}\,\Delta\beta_s, \quad \Delta\omega_i = v_{gi}\,\Delta\beta_i.$$

Since $\Delta\omega_s + \Delta\omega_i$ is a known quantity (which depends on the longitudinal mode distribution of the free resonator), $\Delta\beta_s$ and $\Delta\beta_i$ are not independent but related by

$$\Delta\beta_s v_{gs} + \Delta\beta_i v_{gi} = \Delta\omega_s + \Delta\omega_i.$$

A. Mathematical Model

In the optical waveguide that constitutes the IOPO under examination [14], the electromagnetic field can be written in the form

$$\overline{E}(x, y, z, t) = \sum_k c_k(z)\overline{E}_k(x, y)$$

$$\cdot \exp\left[j(\omega_k t - \beta_k z)\right] + \text{c.c.}$$

where $k = s, i, p$ includes the three parametrically coupled modes, $c_k(z)$ are the corresponding slowly varying amplitudes and $\overline{E}_k(x, y)$ the modal field distributions in the transverse cross section (normalized so that $|c_k|^2$ is the associated power). Coupled mode techniques [4], [15], [16] can be used to convert the Maxwell equations and the nonlinear constitutive relations into a set of differential equations for the coefficient $c_k(z)$. Introducing the normalized amplitudes n_s, n_i, n_p by means of

$$n_s = \sqrt{\frac{\omega_p}{\omega_s}}\,\frac{c_s(z)}{c_{pi}}\,e^{-j\Delta\beta_s z}$$

$$n_i = \sqrt{\frac{\omega_p}{\omega_i}}\,\frac{c_i(z)}{c_{pi}}\,e^{-j\Delta\beta_i z}$$

$$n_p = \frac{c_p(z)}{c_{pi}}\,e^{-j\Delta\beta_o z} \tag{4}$$

With c_{pi} being the incident pump amplitude outside the resonator (Fig. 1), the coupled mode equations read

$$\frac{dn_s}{dz} = -(\alpha_s + j\Delta\beta_s)n_s - j\gamma n_p n_i^*$$

$$\frac{dn_i}{dz} = -(\alpha_i + j\Delta\beta_i)n_i - j\gamma n_p n_s^*$$

$$\frac{dn_p}{dz} = -(\alpha_p + j\Delta\beta_o)n_p - j\gamma n_s n_i. \tag{5}$$

In the preceding equations α_s, α_i, α_p are the corresponding amplitude attenuation coefficients and

$$\Delta\beta_o = \Delta\beta + \Delta\beta_s + \Delta\beta_i.$$

The coupling coefficient γ given by

$$\gamma = \sqrt{\omega_s \omega_i}\, c_{pi} k$$

is proportional to the square root of the incident pump power and to the coefficient

$$k = \epsilon_0 \sum_{lmn} \chi^{lmn} \int\int E_{pl} E_{sm}^* E_{in}^* \, dx \, dy$$

which is connected to the nonlinear material parameter χ^{lmn} and to the overlapping integral of the mode distributions [14]. For IOPO's in indiffused Ti : LiNbO$_3$ waveguides an extensive discussion of fields and overlapping integral optimization (as regards the threshold condition) has been recently reported [14].

Clearly, apart from the normalizations (4) and the choice of the phases in the definition of $c_k(z)$, (5) is completely equivalent to the well-known differential equations of parametric coupling under plane-wave conditions. The most significant difference being the overlap integral appearing in k. As a result most of the extensive literature on the subject can be directly applied to the IOPO. The work of this paper is concerned with a substantial numerical analysis of IOPO for various sets of parameters which define the operating conditions.

Under general conditions, (5) can only be treated numerically. However, it is known from numerical evaluations [13] and from fundamental considerations [6], [17] that, for high Q resonances, the amplitudes of the resonant modes are quite constant along the z direction. In the following section this assumption will be applied to obtain a complete analytical study of the parametric oscillator.

B. Analytical Solution

It will be assumed that at least one of the modes (the signal) is strongly resonant in order to obtain an analytical solution by an iterative procedure which starts from the approximation: $n_s(z) = n_{so} = $ constant. Clearly the system, composed of the two last equations of (5) with $n_s = n_{so}$, must be solved both in the forward and in the backward directions. Only the solution in the forward direction will be briefly discussed as the backward direction

solution is similar. The system of two linear homogeneous differential equations of first order has a solution which can be written in terms of exponentials. By imposing the boundary conditions $n_i(0^+) = n_{io}$, $n_p(0^+) = n_{po}$, they give

$$n_i^+(z) = \left[\frac{\lambda_2 + \alpha_i + j\Delta\beta_i}{\lambda_2 - \lambda_1} n_{io} + \frac{j\gamma n_{so}^*}{\lambda_2 - \lambda_1} n_{po}\right] e^{\lambda_1 z}$$

$$+ \left[\frac{\lambda_1 + \alpha_i + j\Delta\beta_i}{\lambda_1 - \lambda_2} n_{io} + \frac{j\gamma n_{so}^*}{\lambda_1 - \lambda_2} n_{po}\right] e^{\lambda_2 z}$$

$$n_p^+(z) = (\lambda_1 + \alpha_i + j\Delta\beta_i) \left[\frac{\lambda_2 + \alpha_i + j\Delta\beta_i}{j\gamma n_{so}^*(\lambda_1 - \lambda_2)} n_{io}\right.$$

$$\left. + \frac{1}{\lambda_1 - \lambda_2} n_{po}\right] e^{\lambda_1 z}$$

$$- (\lambda_2 + \alpha_i + j\Delta\beta_i) \left[\frac{\lambda_1 + \alpha_i + j\Delta\beta_i}{j\gamma n_{so}^*(\lambda_1 - \lambda_2)} n_{io}\right.$$

$$\left. + \frac{1}{\lambda_1 - \lambda_2} n_{po}\right] e^{\lambda_2 z} \qquad (6)$$

where the eigenvalues λ_1, λ_2 are

$$\lambda_{1,2} = -\frac{(\alpha_i + \alpha_p) + j(\Delta\beta_i + \Delta\beta_0)}{2}$$

$$\pm \sqrt{\left[\frac{(\alpha_i - \alpha_p) + j(\Delta\beta_i - \Delta\beta_0)}{2}\right]^2 - \gamma^2 |n_{s0}|^2}.$$

The solution in the backward direction $n_i^-(z')$, $n_p^-(z')$ has the same form as (6) where the z axis is reversed, $z' = L - z$, and the initial values n_{io} and n_{po} are replaced by $n_i^+(L)$ and $n_p^+(L)$ multiplied by the corresponding reflection coefficients of the output mirror M_2. The only unknown quantities n_{io} and n_{po} are then determined by imposing the longitudinal self-consistency conditions on the pump and idler waves that, written in terms of the normalized variables n, take the form

$$n_{i0} = \Gamma_{i1} n_i^-(z' = L) \exp[-2j(\beta_i - \Delta\beta_i)L]$$

$$n_{p0} = T + \Gamma_{p1} n_p^-(z' = L) \exp[-2j(\beta_p - \Delta\beta_0)L]$$

where Γ_{im}, Γ_{pm} ($m = 1, 2$) are the amplitude reflection coefficients for idler and pump due to the mth mirror, T is the amplitude transmission coefficient of the input mirror at the pump wavelength and takes into account the incident pump wave which, owing to the normalization, has unit amplitude. Taking into account the definition of $\Delta\beta_o$ and of $\Delta\beta_i$ (see Fig. 3), the preceding expressions can be simplified by using the free resonance conditions for idler and signal including the phase of Γ [denoted as arg (Γ)]; one then obtains

$$n_{io} = |\Gamma_{i1}| n_i^-(L) \exp[-j \arg(\Gamma_{i2})]$$

$$n_{po} = T + \Gamma_{p1} n_p^-(L) \exp\{-j[\arg(\Gamma_{s1}) + \arg(\Gamma_{s2})$$

$$+ \arg(\Gamma_{i1}) + \arg(\Gamma_{i2})]\}. \qquad (7)$$

The formal solution of (7) allows one to express n_{io} and n_{po} as functions of n_{so} only. By substituting n_{io} and n_{po} in (6), closed form expressions for the forward ($+$) and the backward ($-$) traveling amplitudes can be written as

$$n_i^+(z) = j\gamma n_{so}^* \overline{K}(K_1 e^{\lambda_1 z} + K_2 e^{\lambda_2 z})$$

$$n_p^+(z) = -\overline{K}[(\lambda_1 + \alpha_i + j\Delta\beta_i)K_1 e^{\lambda_1 z}$$

$$+ (\lambda_2 + \alpha_i + j\Delta\beta_i)K_2 e^{\lambda_2 z}]$$

$$n_i^-(z') = j\gamma n_{so}^* \overline{K}(K_3 e^{\lambda_1 z'} + K_4 e^{\lambda_2 z'})$$

$$n_p^-(z') = -\overline{K}[(\lambda_1 + \alpha_i + j\Delta\beta_i)K_3 e^{\lambda_1 z'}$$

$$+ (\lambda_2 + \alpha_i + j\Delta\beta_i)K_4 e^{\lambda_2 z'}] \qquad (8)$$

where $\overline{K}$, K_1, K_2, K_3, K_4 depend only on the signal level $|n_{so}|$ and on $\Delta\beta_i$ (or $\Delta\beta_s$); explicit expressions for these parameters are given in the Appendix. The last step of the solution process refers to the first of equations (5), which is concerned with the evolution of the signal along the resonator; in the forward direction it reads

$$\frac{dn_s}{dz} = -(\alpha_s + j\Delta\beta_s)n_{so} - j\gamma n_p^+ n_i^{+*}$$

where, for the sake of simplicity, the approximation $n_s = n_{so}$ has been introduced in the right-hand side. The last term of the equation is readily obtained from (8). It is immediately possible to write down the solution in the form

$$n_s^+(z) = n_{so} G_s(z)$$

where the gain at position z is given by

$$G_s(z) = 1 - (\alpha_s + j\Delta\beta_s)z + \gamma^2 |\overline{K}|^2$$

$$\cdot \left[|K_1|^2(\lambda_1 + \alpha_i + j\Delta\beta_i)\right.$$

$$\cdot \frac{\exp(2 \operatorname{Re}\{\lambda_1\}z) - 1}{2 \operatorname{Re}\{\lambda_1\}}$$

$$+ |K_2|^2(\lambda_2 + \alpha_i + j\Delta\beta_i)$$

$$\cdot \frac{\exp(2 \operatorname{Re}\{\lambda_2\}z) - 1}{2 \operatorname{Re}\{\lambda_2\}}$$

$$- K_1 K_2^*(\lambda_1 + \alpha_i + j\Delta\beta_i)$$

$$\cdot \frac{\exp\{\lambda_1 + \lambda_2^*\}z - 1}{\{\lambda_1 + \lambda_2^*\}} +$$

$$- K_1^* K_2(\lambda_2 + \alpha_i + j\Delta\beta_i)$$

$$\cdot \frac{\exp\{\lambda_1^* + \lambda_2\}z - 1}{\{\lambda_1^* + \lambda_2\}}\right]. \qquad (9)$$

By means of a similar procedure, the backward signal wave $n_s^-(z')$ is computed, by using as a starting value at $z' = 0$: $\Gamma_{s2} n_{so} G_s(L)$, where Γ_{s2} is the signal reflection

coefficient of the output mirror. The final expression reads

$$n_s(z') = n_{so} \left\{ G_s(L)\Gamma_{s2} - (\alpha_s + j\Delta\beta_s)z' + \gamma^2 \left| \frac{\overline{K}}{\lambda_1 - \lambda_2} \right|^2 \right.$$

$$\cdot \left[|K_3|^2(\lambda_1 + \alpha_i + j\Delta\beta_i) \right.$$

$$\cdot \frac{\exp(2\,\mathrm{Re}\,\{\lambda_1\}z') - 1}{2\,\mathrm{Re}\,\{\lambda_1\}}$$

$$+ |K_4|^2(\lambda_2 + \alpha_i + j\Delta\beta_i) \frac{e^{2\mathrm{Re}\{\lambda_2\}z'} - 1}{2\,\mathrm{Re}\,\{\lambda_2\}}$$

$$- K_3 K_4^*(\lambda_1 + \alpha_i + j\Delta\beta_i)$$

$$\cdot \frac{\exp\{\lambda_1 + \lambda_2^*\}z' - 1}{\{\lambda_1 + \lambda_2^*\}}$$

$$- K_3^* K_4(\lambda_2 + \alpha_i + j\Delta\beta_i)$$

$$\left. \left. \cdot \frac{\exp\{\lambda_1^* + \lambda_2\}z' - 1}{\{\lambda_1^* + \lambda_2\}} \right] \right.$$

$$= n_{so} G_s'(z') \qquad (10)$$

which implicitly defines the backward gain function $G_s'(z')$.

The final equation of the model is the longitudinal self-consistency condition for the signal which, after some simple consideration like those leading to (7), can be written in the form

$$|\Gamma_{s1}| G_s'(L) \exp[-j \arg(\Gamma_{s2})] = 1. \qquad (11)$$

It is important to observe that this complex equation contains only two real unknowns [through the function $G_s'(L)$, see (10): $|n_{so}|^2$ and $\Delta\beta_i$ (or $\Delta\beta_s$)] and is independent of the phase of n_{so}. So both signal level (corresponding to a certain value of the incident pump power) and working frequency (through the shift from the nearest free-cavity resonance, see Fig. 3) are completely determined by the solution of (11).

III. NUMERICAL SIMULATION

The model developed here has two advantages with respect to a fully numerical one; it is general and analytically compact. This allows, within the limits of the model itself, an exhaustive study of parametric oscillator performance without the associated computational effort that a full numerical approach would require. The main limits of the model are the "constant signal" approximation and the monochromatic pump-wave assumption. The first condition requires high mirror reflectivities and small propagation losses for the signal wave, both obtainable using Ti:LiNbO₃ technology. The last condition is satisfied by using a pump source with a linewidth smaller than the difference in free spectral range at signal and idler wavelengths [13], [18]. Typical parameter values [14] are reported in Table I. Except when explicitly stated, these values have been adopted in the numerical simulations.

TABLE I
TYPICAL PARAMETER VALUES USED IN THE
SIMULATIONS

$\lambda_s = 1.120\ \mu m$
$\lambda_p = 0.587\ \mu m$
$v_{gs} = 1.306 \cdot 10^8\ m/s$
$v_{gi} = 1.312 \cdot 10^8\ m/s$
$v_{gp} = 1.241 \cdot 10^8\ m/s$
$\alpha_s = \alpha_i = 0.03\ dB/cm$
$\alpha_p = 0.09\ dB/cm$
$L = 4.31\ cm$
$R_s = R_i = 0.986$

In what follows, the most significant results concerning IOPO operation obtained during the course of this study, will be described. Operating frequency, threshold pump power and maximum conversion efficiency will be discussed in the three typical configurations in which the DRO (doubly resonant oscillator) or the SRO (singly resonant oscillator) may work. They are known as single pass (SP; $\Gamma_{p1} = \Gamma_{p2} = 0$), double pass (DP; $\Gamma_{p1} = 0$, $|\Gamma_{p2}| \neq 0$), and resonant pump case (RP; $|\Gamma_{p1}| \neq 0$, $|\Gamma_{p2}| \neq 0$). The value of the pump reflectivity $|\Gamma_{pm}|$ is usually high in DP or RP operation, but in practice also the case with low $|\Gamma_{pm}|$ is relevant because it allows simulation of actual SP-IOPO operation conditions. Until now only SP-IOPO's have been built, and so in the following we will use $|\Gamma_{pm}| = 0.5$, except when explicitly stated, to estimate the effect on the operation conditions of a residual reflectivity due to signal and idler mirrors at the pump wavelength.

The particular attention devoted to the DRO is a result of the possibility them being fabricated [12], [13] and the interest in the evolutionary behavior to the SRO condition.

A. Operating Frequency

It has been shown [2], [13] that, if signal and idler waves have the same losses $\alpha_i = \alpha_s$ and power mirror reflectivities $R_i = R_s$, the oscillator operating point is perfectly symmetrical in the β scales so that

$$\Delta\beta_s = \Delta\beta_i$$

holds independently of the incident pump power. Now the symmetry assumptions are dropped, letting idler power reflectivity R_i at both mirrors reduce until SRO operating condition is achieved ($R_i = 0$). Supposing monomode operation during the transition to SRO operation, a continuous shifting of the emission frequency can be observed and, in the final condition, it is near signal resonance on the opposite side with respect to synchronism ($\Delta\beta = 0$).

When R_i is diminishing, the evolution of the operating point depends on the phase mismatch $\Delta\beta$. In particular the larger is $\Delta\beta$ the faster is the spectral line displacement from the signal resonant mode. At phase matching the

movement stops just on the resonance (in this case SRO operating frequency is that of a free-cavity mode). Finally, when signal and idler resonances are not identical, the emission frequency depends on incident pump power. Clearly these results for the SRO hold until the hypothesis of single frequency operation ceases to be valid. In the SRO regime the operation is multimode and the previous resutls can be qualitatively extrapolated for the frequency behavior of each oscillating mode.

B. Pump Threshold Power and Maximum Efficiency

In this section we vary the main parameters (mirror reflectivities $\Delta\beta$, $\Delta\beta_s$) and present the behavior of the following quantities: threshold pump power and maximum signal efficiency (maximum at varying incident pump power). In order to have normalized pump powers, in all the following diagrams the variable P_{th} has been introduced, where

$$P_{\text{th}} = \frac{|c_{pi}|^2}{P_{\text{th}o}}$$

and $P_{\text{th}o}$ is the minimum threshold pump power of a symmetrical SP DRO with $R_s = R_i = 0.986$. The numerical value of $P_{\text{th}o}$ depends on several parameters (see Table I) including the overlapping integral which appears in k (for its evaluation see [14]); good theoretical values can be in the order of mW [14], while experimental values can be near to tens of mW [19]. The signal efficiency is, in the following, defined as the ratio between the output signal power (beyond the output mirror M_2) and the input pump power (before the input mirror M_1) expressed as a percentage

$$\eta = \frac{\omega_p}{\omega_s} |n_{so}|^2 (1 - R_s) 100$$

where the approximation $n_s(z) \cong n_{so}$ has been used.

As a first example, under phase matching conditions ($\Delta\beta = \Delta\beta_s = 0$), the transition from DRO to SRO (Fig. 4) and from SP to DP (Fig. 5) as regards the threshold power and the maximum efficiency η_M variation have been computed. In both cases the phases due to mirror reflections have been assumed equal to zero. In the following sections we will discuss the effect of the relative phase changes, after mirror reflection, on the interaction efficiency. Simulations show how DP operation improves oscillator performances for both threshold and efficiency.

Transition from SP to RP is illustrated in Fig. 6 where the moduli of pump reflection coefficients are assumed equal for both mirrors. The threshold decreases considerably as is expected and the maximum efficiency is almost constant until

$$0 \leq |\Gamma_{p1}| = |\Gamma_{p2}| \leq 0.7.$$

Beyond this point a further increase in the mirror reflectivities requires a higher proportion of the system energy to support the pump resonant wave and hence the efficiency sharply decreases. It is interesting to observe that
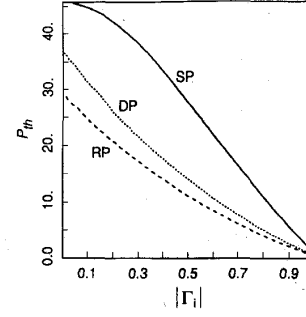

Fig. 4. Behavior of threshold power normalized with respect to $P_{\text{th}o}$ (P_{th}) in the transition from DRO to SRO (———: SP; · · · · · ·: DP; - - - - -: RP).
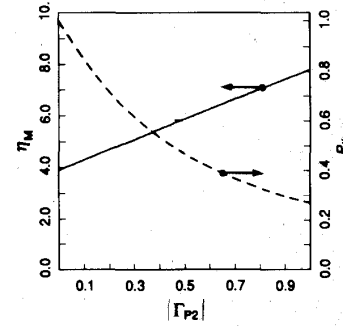

Fig. 5. Behavior of normalized threshold power P_{th} and maximum efficiency conversion η_M in the transition from SP to DP.
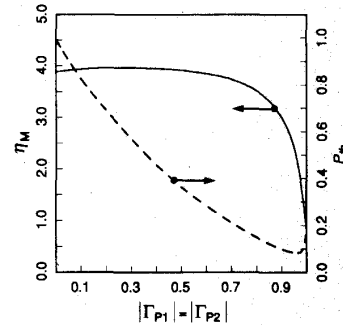

Fig. 6. As Fig. 5 in the transition from SP to RP with $\Delta\beta_s = \Delta\beta = 0$ and arg (Γ_{sm}) = arg (Γ_{im}) = 0.

the RP operation does not improve the maximum efficiency with respect to the SP case. This is due to the fact that, in the RP case, the conditions which minimize threshold power differ from those which optimize efficiency as will be shown later.

Finally, the effect on threshold and on maximum efficiency of a decrease in the power reflection coefficient for signal and idler waves has been considered. The lower range of the reflectivity has been limited to 0.75 so as not to invalidate the constant signal assumption. Some results are shown in Fig. 7.

An examination of Figs. 5–7 shows that a working condition close to the efficiency-"knee" represents a good
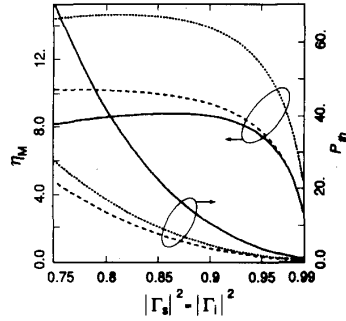
Fig. 7. Effect on threshold and maximum efficiency of a decrease of the reflection coefficient modulus for signal and idler waves (———: SP; ·········: DP; -----: RP).
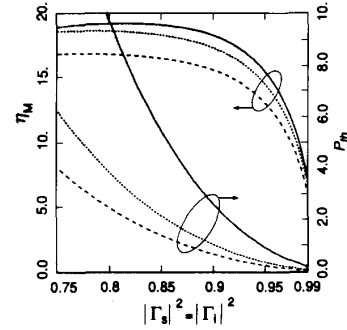

Fig. 8. Effect on threshold and maximum efficiency of a decrease of reflection coefficient modulus for signal and idler waves with a fixed pump reflectivity at M_2 ($|\Gamma_{p2}|^2 = 0.986$) and three different values at M_1 (———: $|\Gamma_{p1}|^2 = 0$; ····: $|\Gamma_{p1}|^2 = 0.25$; ---: $|\Gamma_{p1}|^2 = 0.5$).

compromise between low threshold and satisfactory device efficiency. If the highest obtainable efficiencies of the DRO are desired, it is necessary to work with

$$|\Gamma_{p2}| \cong 1, \quad 0.8 \leq R_s \leq 0.9$$

to ensure that the threshold powers are reasonable. Fig. 8 shows the maximum efficiency and the threshold versus $|\Gamma_s|^2 = |\Gamma_i|^2$ for $|\Gamma_{p2}|^2 = 0.986$ and for three different values of $|\Gamma_{p1}|^2$. From the previous figures it can be seen that it is possible to have efficiency up to 20%, albeit with higher thresholds. If the input mirror presents a residual reflectivity to the pump wave, an improved compromise between low threshold power and high efficiency can be achieved. In fact, threshold becomes appreciably lower than in the double-pass case while maximum efficiency is not greatly reduced. For example, with $R_s = 0.9$ a maximum efficiency of about 18% is achieved with a reasonably low threshold pump power increase for $|\Gamma_{p1}|^2 = 0.25$.

C. Effect of $\Delta\beta_s$

After having studied how the interaction depends on the mirror reflectivities for the three waves, the role of the phase parameters has been considered. With respect to $\Delta\beta_s$ (see Fig. 3), the analysis of the results has shown that in order to have low threshold power the condition $\Delta\beta_s = \Delta\beta_i = 0$ is absolutely general independent of the values of the other parameters and of the chosen oscillator configuration. The alignment of the signal and idler resonances (Fig. 3) is a highly advantageous condition for initiating oscillation. However, the conversion efficiency maximized with respect to the pump power (η_M) shows a peak for $\Delta\beta_s = \Delta\beta_i = 0$ only in phase matched conditions ($\Delta\beta = 0$) or if $\Delta\beta \neq 0$, with an optimum choice of the relative phase reflections of the mirrors. In the absence of these conditions the peak of the maximized efficiency appears, with a proper choice of mirror phases, on the side of the resonance alignment (center of the cluster) towards the phase matching condition. Examples of results for a DRO–SP are shown, with $\Delta\beta L$ as a parameter in Fig. 9.
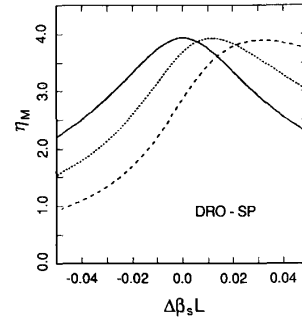

Fig. 9. Dependence of maximized conversion efficiency (with respect to the pump power) on $\Delta\beta_s L$ in a DRO–SP (———: $\Delta\beta L = 0$; ·········: $\Delta\beta L = 1.5$; -------: $\Delta\beta L = 3$).

D. Effect of Mirror Phase Shifts

It is now interesting to investigate the interaction dependence on the phase shifts due to the mirrors and on the phase mismatch $\Delta\beta$. They are related to each other since the effects of the phase shifts introduced at the reflection modify the preexisting phase relations between the waves. An important result obtained from the model is that the oscillator performance does not depend on the absolute phase shifts due to the mirrors, but depends (and not in every configuration) on the relative phase shifts introduced by the mirrors between the three waves, i.e., on the variables

$$\phi_{rel}^{(1)} = \arg(\Gamma_{p1}) - \arg(\Gamma_{s1}) - \arg(\Gamma_{i1})$$

$$\phi_{rel}^{(2)} = \arg(\Gamma_{p2}) - \arg(\Gamma_{s2}) - \arg(\Gamma_{i2})$$

for the first and second mirror, respectively. This result reduces the number of parameters in the simulations. In Table II the dependence of the threshold and efficiency on the quantities $\phi_{rel}^{(1)}$ and $\phi_{rel}^{(2)}$ in the various kinds of oscillator configurations is summarized.

As is obvious, some configurations are independent of the relative phase and so the interaction is not influenced by the phase shifts at the mirrors. This is physically reasonable if one considers that for each reflection there is

TABLE II
OSCILLATOR CHARACTERISTICS DEPENDENCE OF THE VARIOUS
CONFIGURATIONS ON THE RELATIVE PHASE-SHIFTS $\phi_{rel}^{(1)}$ AND $\phi_{rel}^{(2)}$

	DRO	SRO
SP	no dependence	no dependence
DP	dependence on $\phi_{rel}^{(2)}$	no dependence
RP	dependence on $\phi_{rel}^{(1)} +$ $\phi_{rel}^{(2)}$, $\phi_{rel}^{(2)}$	dependence on $\phi_{rel}^{(1)} +$ $\phi_{rel}^{(2)}$

always, in the examined cases, at least one wave whose phase is free, i.e., in a certain sense, it can determine itself. On the other hand, if we examine, for instance, a DRO-DP, only the pump at the first mirror (at $z = 0^+$) can freely choose its phase while at the second mirror all three waves have their phases fixed which explains why a dependence on the parameter $\phi_{rel}^{(2)}$ exists. If the pump resonates, the interaction depends also on the quantity $\phi_{rel}^{(1)} + \phi_{rel}^{(2)}$ that is related to the more or less good pump resonance (at fixed $\Delta\beta$). Analytical results have been obtained in the case of symmetry between signal and idler with respect to the mirror reflectivities and the attenuation coefficients. The optimum $\Delta\beta$, $\phi_{rel}^{(1)}$, $\phi_{rel}^{(2)}$ conditions with respect to the threshold are shown below for every kind of DRO oscillator

$$\text{SP: } \Delta\beta_o = 0$$

$$\text{DP: } \Delta\beta_o = 0, \quad \phi_{rel}^{(2)} = \Delta\beta_o L + 2k\pi$$

$$\text{RP: } \Delta\beta_o = 0, \quad \phi_{rel}^{(2)} = \Delta\beta_o L + 2k\pi,$$

$$\phi_{rel}^{(1)} + \phi_{rel}^{(2)} = 2\Delta\beta_o L + 2k\pi \qquad (12)$$

where $\Delta\beta_o = \Delta\beta + \Delta\beta_s + \Delta\beta_i$. For the SP it follows that the lowest pump threshold is obtained when $\Delta\beta = 0$, since $\Delta\beta_s$ and $\Delta\beta_i$ are very small quantities. In the other two cases, if $\phi_{rel}^{(1)}$ and $\phi_{rel}^{(2)}$ are different from zero, there will be a value $\Delta\beta_{opt}$ (generally not zero) that minimizes the threshold. From the second equation of (12) it follows that, in the DP case

$$0 \le |\Delta\beta_{opt}L| \le \pi$$

while in a RP configuration

$$0 \le |\Delta\beta_{opt}L| \le \pi/2$$

it being numerically proved that the third condition given in (12) is stronger than the second. This means that, when both mirrors reflect the pump, the threshold and consequently the working frequencies are more strongly determined by phase matching than in a DP. The worst conditions for the DRO threshold are

$$\text{SP: } \Delta\beta_o L = 2k\pi \quad k \neq 0$$

$$\text{DP: } \Delta\beta_o L = \phi_{rel}^{(2)} + (2k + 1)\pi$$

$$\text{RP: } \Delta\beta_o L = \phi_{rel}^{(2)} + (2k + 1)\pi,$$

$$2\Delta\beta_o L = \phi_{rel}^{(1)} + \phi_{rel}^{(2)} + (2k + 1)\pi.$$
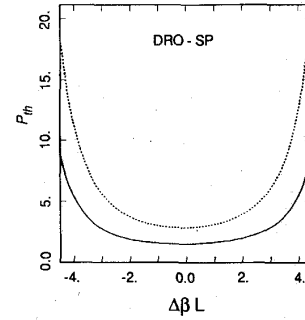

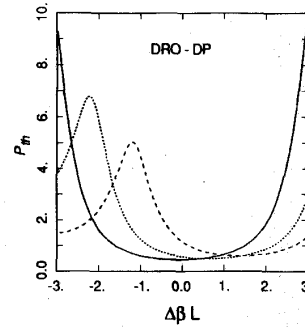Fig. 10. Dependence of threshold power on the phase mismatch in a DRO-SP (———: $\Delta\beta_s L = 0$; $\cdots\cdots\cdots$: $\Delta\beta_s L = 0.025$).

Fig. 11. As Fig. 10 in DRO-DP oscillators with (———: $\phi_{rel}^{(2)} = 0$; $\cdots\cdots\cdots$: $\phi_{rel}^{(2)} = 1$; ———–: $\phi_{rel}^{(2)} = 2$).

The general behavior can be observed in Figs. 10–12 for SP, DP, and RP, respectively. The numerical results show that, in SP and DP, the conditions to minimize threshold are not very far from those that maximize the efficiency, while in a resonant pump configuration there is a trade off between these two requirements. The condition of absolute maximum efficiency is obtained as the solution of one of the following relations

$$\Delta\beta L = \phi_{rel}^{(1)} \pm \pi$$

and the minimums as the solutions of

$$\Delta\beta L - \phi_{rel}^{(1)} = 2k\pi.$$

Fig. 13 represents η_M versus $\phi_{rel}^{(1)}$ with $\Delta\beta L$ as a parameter and is in good agreement with the previous conditions.

E. Effect of Phase Mismatch on Signal Efficiency

Recent experimental results [19] showed for the DRO a monomodal emission in low pump power regime (single-cluster operation) whereas emissions with more than one spectral output line are possible if the incident pump power is increased. Since single mode emission is very advantageous in a lot of applications, it would be interesting to evaluate the behavior of the device, in its different configurations, to allow single-cluster operation. For this condition conversion efficiency versus phase mis-
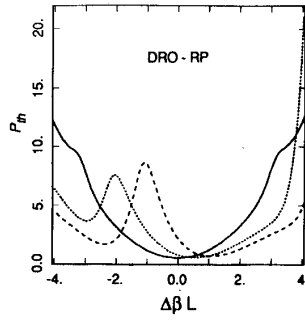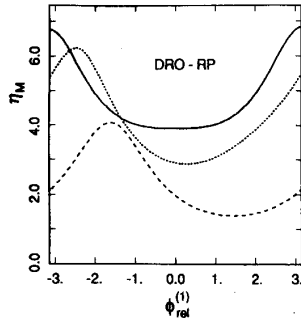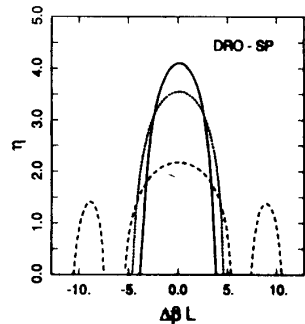
Fig. 12. As Fig. 10 for DRO–RP oscillators.

Fig. 15. As in Fig. 14 in DRO–DP oscillators.

Fig. 13. Dependence of maximum conversion efficiency on $\phi_{rel}^{(1)}$ in a DRO–RP (———: $\Delta\beta L = 0$; ············: $\Delta\beta L = 1$; ------: $\Delta\beta L = 2$) for $\phi_{rel}^{(2)} = 0$.
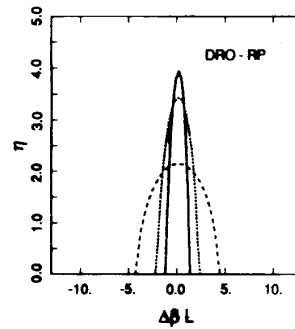
Fig. 16. As in Fig. 14 in DRO–RP oscillators.

Fig. 14. Curves of conversion efficiency versus phase mismatch in a DRO–SP; the three curves are related to different pump power levels above minimum threshold (———: pump power four times above threshold; ············: ten times; ------- forty times).

match is investigated. The analysis has been performed under the condition of perfect resonance alignment $\Delta\beta_s = \Delta\beta_i = 0$ at every operating point. Figs. 14–16 represent the results for SP, DP, and RP, respectively, at three different relative values of input pump level. This level is referred to the corresponding threshold evaluated, in each case, for the $\Delta\beta = 0$ condition.

From the figures it can be seen that the allowed mismatch interval broadens with increasing pump power, increasing the band into which the oscillations can start up. It is known that emission is connected to the occurrence
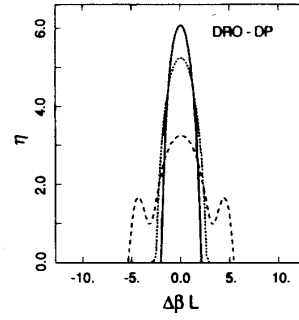
of clusters, separated by $|\Delta\beta L| = \pi$. The comparison of this quantity with the efficiency bandwidth (Figs. 14–16) allows the possibility of single frequency emission to be predicted. Such a condition is difficult to obtain in SP devices while it is favored by DP and more so by RP, which is the actual configuration under consideration.

These curves allow quantitative interpretation of the experimental behavior of an actual DRO obtained when the operating point is changed through variation of the pump wavelength [20]. A comparison between the device bandwidths shows that the allowed SP bandwidth at four times above its threshold is almost equal to that of the RP operating forty times above its reference threshold although the pump wave is scarcely resonant ($|\Gamma_{p1}|^2 = |\Gamma_{p2}|^2 = 0.25$). Transition from DRO to SRO (by decreasing $|\Gamma_i|^2$) makes the bandwidth change in a singular way, especially for DP and RP. That is for $|\Gamma_i|^2 > 0.25$ the bandwidth does not suffer appreciable variation in comparison with the DRO condition, while for the SRO condition ($|\Gamma_i| = 0$) the bandwidth is almost doubled in a DP operation and is increased to three times in a RP operation. In practice it becomes the same for all three configurations as shown in Fig. 17. It is known that, approaching SRO operation, the oscillator loses its intrinsic monomodal emission (derived from the cluster effect) and shows a continually broadening output spectrum. Therefore, one can reasonably predict that the SRO emission spectrum will be located around the absolute maximum of the available bandwidth in Fig. 17.
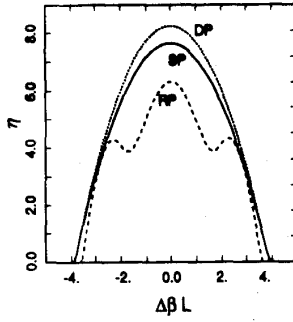
Fig. 17. Curves of conversion efficiency versus phase mismatch in a SRO; the three curves are related to different configurations (———: SP; ·············: DP; ‑‑‑‑‑‑‑‑: RP) with each pump power level fixed at four times its own threshold for $\Delta\beta = 0$.

Fig. 19. Boundary curves for hysteresis in $\Delta\beta - \Delta\beta_s$ plane (———: SP, ·············: DP with $|\Gamma_{p2}|^2 = 0.25$, ‑‑‑‑‑‑‑: DP with $|\Gamma_{p2}|^2 = 0.986$).
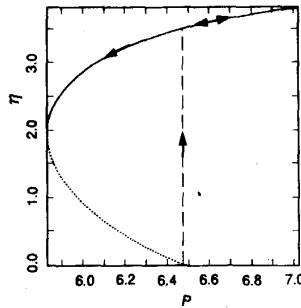

Fig. 18. Example of hysteretic behavior: SP device characteristic corresponding to point A in Fig. 19. The pump power is normalized with respect to P_{tho}.

tical cavity parameters. The analysis is based on an almost completely analytical model whose validity is quite general and that overcomes the problems of a completely numerical solution. Particular attention has been devoted to the transition from the doubly to the singly resonant condition in order to estimate the difference in the required optical pump powers and also to determine the region of possible hysteretic behavior.

IV. HYSTERESYS

The model implemented has allowed, for the various DRO, determination of working conditions which give rise to hysteresis in the efficiency curve versus normalized pump power. An example of the behavior considered is shown in Fig. 18.

This analysis has allowed generalization of the studies of these behaviors reported in [21]. Hysteresis phenomena have been shown in operating conditions far from the phase matching condition and resonance alignment and then also far from the minimum pump threshold level. Hysteresis phenomena are allowed only if the condition $(\Delta\beta_s \Delta\beta) > 0$ is satisfied. In Fig. 19 the curves show the boundary of the region where hysteretic behavior can occur in the three operating conditions. The shape of the hysteresis curve changes drastically in the hysteretic region and it becomes more pronounced as $(\Delta\beta_s L \, \Delta\beta L)$ increases, which induces a greatly increased threshold power. As an example, a SP-DRO operating at point A in Fig. 19 yields the response curve of Fig. 18.

V. CONCLUSION

In this paper an extensive analysis has been carried out on the static characteristics of integrated optics parametric oscillators in their various configurations, varying the op-
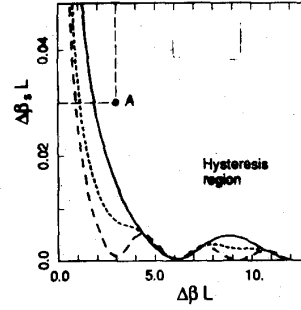
APPENDIX

By a simple, but lengthy, manipulation of the longitudinal self consistency relations one obtains

$$\overline{K} = \frac{T}{(\lambda_1 - \lambda_2)(c_1 c_4 - c_2 c_3)}$$

$$K_1 = (\lambda_2 + \alpha_i + j\Delta\beta_i)c_2 - c_1$$

$$K_2 = (\lambda_1 + \alpha_i + j\Delta\beta_i)c_2 - c_1$$

$$K_3 = \Gamma_{i2}(\lambda_2 + \alpha_i + j\Delta\beta_i)(\overline{A}c_2 - \overline{B}c_1)$$
$$\quad + \Gamma_{p2}(\overline{C}c_2 - \overline{D}c_1)$$

$$K_4 = \Gamma_{i2}(\lambda_1 + \alpha_i + j\Delta\beta_i)(\overline{A}c_2 - \overline{B}c_1)$$
$$\quad + \Gamma_{p2}(\overline{C}c_2 - \overline{D}c_1)$$

with

$$c_1 = 1 - \frac{|\Gamma_{i_1}| \exp\left[-j \arg(\Gamma_{i_2})\right]}{(\lambda_1 - \lambda_2)^2}[\Gamma_{i_2}\overline{A}^2 + \Gamma_{p2}\overline{B}\,\overline{C}]$$

$$c_2 = -\frac{|\Gamma_{i_1}| \exp\left[-j \arg(\Gamma_{i_2})\right]}{(\lambda_1 - \lambda_2)^2}\overline{B}[\Gamma_{i_2}\overline{A} + \Gamma_{p2}\overline{D}]$$

$$c_3 = -\frac{\Gamma_{p_1} \exp\left\{-j[\arg(\Gamma_{i_1}\Gamma_{i_2}\Gamma_{s_1}\Gamma_{s_2})]\right\}}{(\lambda_1 - \lambda_2)^2}\overline{C}[\Gamma_{i_2}\overline{A} + \Gamma_{p2}\overline{D}]$$

$$c_4 = 1 - \frac{\Gamma_{p_1} \exp\left\{-j[\arg(\Gamma_{i_1}\Gamma_{i_2}\Gamma_{s_1}\Gamma_{s_2})]\right\}}{(\lambda_1 - \lambda_2)^2}$$
$$[\Gamma_{i_2}\overline{B}\,\overline{C} + \Gamma_{p2}\overline{D}^2]$$

and

$$\overline{A} = (\lambda_1 + \alpha_i + j\Delta\beta_i)e^{\lambda_2 L} - (\lambda_2 + \alpha_i + j\Delta\beta_i)e^{\lambda_1 L}$$

$$\overline{B} = e^{\lambda_2 L} - e^{\lambda_1 L}$$

$$\overline{C} = (\lambda_1 + \alpha_i + j\Delta\beta_i)(\lambda_2 + \alpha_i + j\Delta\beta_i)(e^{\lambda_1 L} - e^{\lambda_2 L})$$

$$\overline{D} = (\lambda_1 + \alpha_i + j\Delta\beta_i)e^{\lambda_1 L} - (\lambda_2 + \alpha_i + j\Delta\beta_i)e^{\lambda_2 L}$$

ACKNOWLEDGMENT

REFERENCES

[1] J. A. Armstrong, N. Bloembergen, J. Ducuing, and P. S. Pershan, "Interactions between light waves in a nonlinear dielectric," *Phys. Rev.*, vol. 127, pp. 1918–1939, 1962.

[2] G. D. Boyd and A. Ashkin, "Theory of parametric oscillator threshold with single-mode optical masers and observation of amplification in LiNbO₃," *Phys. Rev.*, vol. 146, pp. 187–198, 1966.

[3] S. E. Harris, "Tunable optical parametric oscillation," in *Proc. IEEE*, vol. 57, pp. 2096–2113, 1969.

[4] W. Sohler, "Second order nonlinear guided wave interaction," in *Nonlinear Surface Electromagnetic Phenomena*, H. E. Ponath and G. Stegeman, Eds. New York: Elsevier Science, 1990, ch. 1.

[5] H. Suche and W. Sohler, "Integrated optical parametric oscillators," *J. Optoelectron. Dev. and Technol.*, vol. 4, pp. 1–20, 1989.

[6] R. L. Byer, "Optical parametric oscillators," in *Quantum Electronics*, vol. 1, part B, H. Rabin and C. L. Tang, Eds. New York: Academic, 1975.

[7] R. G. Smith, "Optical parametric oscillators," in *Laser Handbook*, vol. 1, Arecchi and Schuls-Dubois, Eds. Amsterdam: North Holland, 1972.

[8] ——, "Optical parametric oscillators," in *Advances in Lasers*, vol. 4, Levine and De Maria, Eds. New York: Dekker, 1976.

[9] R. L. Byer, "Parametric oscillators and nonlinear material," in *Nonlinear Optics*, Harper and B.S., Eds. San Francisco, CA: Academic, 1977.

[10] R. G. Smith, "A study of factors affecting the performance of a continuously pumped doubly resonant optical parametric oscillator," *IEEE J. Quantum Electron.*, vol. QE-9, pp. 530–540, 1973.

[11] J. A. Giordmaine and R. C. Miller, "Optical parametric oscillation in LiNbO₃," *Physics of Quantum Electronics*, Kelly, Lax, and Tannenwald, Eds. New York: McGraw-Hill, 1965.

[12] H. Suche, H. Teichmann, and W. Sohler, "Single frequency operation of doubly resonant integrated optical parametric oscillators," presented at First Euro. Quantum Electron. Conf., EQEC'88, Hannover, Germany, 1988, paper WeBB3.

[13] G. P. Bava, I. Montrosset, and R. Pelissero, "Numerical modeling of integrated optics doubly resonant parametric oscillators," in *Nonlinear Guided-Wave Phenomena: Physics and Applications*, Houston, TX, vol. 2, 1989, pp. 84–87, paper THB18.

[14] G. P. Bava, I. Montrosset, W. Sohler, and H. Suche, "Numerical modeling of Ti:LiNbO3 integrated optical parametric oscillators," *IEEE J. Quantum Electron.*, vol. QE-23, pp. 42–51, 1987.

[15] D. Marcuse, *Theory of Dielectric Optical Waveguides*. New York: Academic, 1974.

[16] W. Sohler, "Nonlinear integrated optics," in *NATO Asi Series E, New Directions in Guided Wave and Coherent Optics*. D. B. Ostrowsky and E. Spitz, Ed., vol. II, 1984, pp. 449–480.

[17] W. Brunner and H. Paul, "Theory of optical parametric amplification and oscillation," in *Progress in Optics*, vol. 15, E. Wolf, Ed. New York: Elsevier North-Holland, 1977, pp. 3–73.

[18] J. E. Björkholm, "Some spectral properties of doubly and singly resonant pulsed optical parametric oscillators," *Appl. Phys. Lett.*, vol. 13, pp. 399–401, 1968.

[19] H. Suche and W. Sohler, "Single frequency pumped doubly resonant integrated optical parametric oscillator of very high efficiency," *Integrated and Guided-Wave Optics*, IGWO'88, Santa Fé, NM, 1988, vol. 5, pp. 176–180, paper MF15.

[20] G. P. Bava, I. Montrosset, R. Pelissero, W. Sohler, and H. Suche, "Spectral and temporal development of the emission of a doubly resonant integrated optical parametric oscillator," in *Proc. SPIE, ECIO'89*, Paris, vol. 1141, pp. 26–31, 1989.

[21] L. A. Lugiato, C. Oldano, C. Fabre, E. Giacobino, and R. J. Horowicz, "Bistability, self-pulsing and chaos in optical parametric oscillators," *Il Nuovo Cimento*, vol. D10, pp. 959–970, 1988.

G. Colucci, photograph and biography not available at the time of publication.

D. Romano, photograph and biography not available at the time of publication.

Gian Paolo Bava was born in Varallo, Italy, in 1937. He received the degree in electrical engineering from Politecnico di Torino, Torino, Italy, in 1961.

Since 1961 he has been with, successively, the Institute of Electrical Communications and the Department of Electronics, Politecnico di Torino. From 1970 to 1976 he was in charge of a course on microwave techniques in the Department of Electronics. Currently his main research interests are in microwave mesfet amplifiers and oscillators and integrated optics.

Ivo Montrosset was born in Aosta, Italy, in 1946. He received the degree in electronic engineering (laurea) from the Politecnico di Torino, Italy in 1971.

He was with the Department of Electronics, Politecnico di Torino, from 1972 to 1986. In 1982 he became an Associate Professor. In June 1986 he was appointed Full Professor with the Department of Biophysics and Electronics, University of Genova, Genova, Italy. In 1990 he rejoined the Department of Electronics, Politecnico di Torino. His main interests are in the field of numerical methods for wave propagation and guided-wave optics.